The Astrophysical Journal, 890:172 (9pp), 2020 February 20 https://doi.org/10.3847/1538-4357/ab6deb

Assessment of Systematic Uncertainties in the Cosmological Analysis of the SDSS Supernovae Photometric Sample

Brodie Popovic[1], Dan Scolnic[1], and Richard Kessler[2,3]
[1] Department of Physics, Duke University, Durham, NC, 27708, USA; brodie.popovic@duke.edu
[2] Department of Astronomy and Astrophysics, The University of Chicago, Chicago, IL 60637, USA
[3] Kavli Institute for Cosmological Physics, University of Chicago, Chicago, IL 60637, USA
Received 2019 October 14; revised 2019 December 29; accepted 2020 January 16; published 2020 February 26

Abstract

Improvements to the precision of measurements of cosmological parameters with Type Ia supernovae (SNe Ia) are expected to come from large photometrically identified (photometric) supernova (SN) samples. Here we reanalyze the Sloan Digital Sky Survey (SDSS) photometric SN sample, with roughly 700 high-quality, likely but unconfirmed SNe Ia light curves, to develop new analysis tools aimed at evaluating systematic uncertainties on the dark energy equation-of-state parameter w. Since we require a spectroscopically measured host-galaxy redshift for each SN, we determine the associated selection efficiency of host galaxies in order to simulate bias corrections. We determine that the misassociation rate of host galaxies is 0.6%; ignoring this effect in simulated bias corrections leads to a w-bias of $\Delta w = +0.0007$, where w is evaluated from SNe Ia and priors from measurements of baryon acoustic oscillations and the cosmic microwave background. We assess the uncertainty in our modeling of the host-galaxy selection efficiency and find the associated w uncertainty to be -0.0072. Finally, we explore new core-collapse (CC) models in simulated training samples and find that adjusting the CC luminosity distribution to be in agreement with previous Pan-STARRS analyses yields a better match to the SDSS data. The impact of ignoring this adjustment is $\Delta w = -0.0109$; the impact of replacing the new CC models with those used by Pan-STARRS is $\Delta w = -0.0028$. These systematic uncertainties are subdominant to the statistical constraints from the SDSS sample, but must be considered in future photometric analyses of large SN samples such as those from the Dark Energy Survey (DES), the Large Synoptic Survey Telescope (LSST), and the Wide Field Infrared Survey Telescope (WFIRST).

Unified Astronomy Thesaurus concepts: Type Ia supernovae (1728); Cosmology (343); Dark energy (351)

1. Introduction

The discovery of accelerating cosmic expansion (Riess et al. 1998; Perlmutter et al. 1999) from measurements of 10 s of Type Ia supernovae (SNe Ia) galvanized a new era in the study of cosmology. In the time since this discovery, collections of 100 s of spectroscopically confirmed SNe Ia have been used to measure the expansion history of the universe up to $z = 1$ (Conley et al. 2011; Betoule et al. 2014; Scolnic et al. 2018; Abbott et al. 2019). A combination of constraints from SNe Ia and those from other probes such as baryon acoustic oscillations (BAO; Eisenstein et al. 2005; Anderson et al. 2014) and the cosmic microwave background (CMB; Bennett et al. 2003; Planck Collaboration et al. 2016a) can be used to infer the dark energy equation-o- state parameter $w = P/\rho\, c^2$, where P is the pressure and ρ is the energy density. The most precise of these measurements is that of Scolnic et al. (2018; hereafter S18), which used 1048 spectroscopically confirmed SNe Ia. Measurements of SNe Ia, combined with constraints from Planck Collaboration et al. (2016b), yield $w = -1.026 \pm 0.041$.

Significant improvements in the constraints on dark energy from supernovae (SNe) require a large jump in the SN sample size. Unfortunately, obtaining such a large number of spectroscopic confirmations for SNe is unfeasible with expected resources in the next decade. Time constraints limit single-object spectroscopy, and the sparse density of SNe ($10\,\mathrm{yr}^{-1}\,\mathrm{deg}^{-2}$ with R-band magnitude <22) makes the yield for multi-object spectroscopy similarly low. On the other hand, spectroscopic classification may not be necessary if one can use photometric classification of the light-curve sample. The difficulty of photometric analysis is that it is susceptible to contamination from core-collapse (CC) SNe and possible contamination from peculiar SNe Ia and non-SN transients such as active galactic nucleus (Campbell et al. 2013; Jones et al. 2018a). Significant effort has been made in classification algorithms (e.g., PSNID—Sako et al. 2008, SuperNNova—Möller & de Boissière 2020, Nearest Neighbour—Kessler & Scolnic 2017, and machine learning methods—Lochner et al. 2016), spurred on by the advent of Pan-STARRS (PS1; Jones et al. 2018a), Dark Energy Survey (DES; Bernstein et al. 2012), Large Synoptic Survey Telescope (LSST; Ivezić et al. 2019), and other SN surveys.

The first cosmological measurement of w with primarily photometric classification was done by Campbell et al. (2013). CC contamination was reduced using the PSNID Bayesian light-curve classifier (Sako et al. 2011), resulting in a final sample with 3.9% CC SNe contamination, as predicted by rigorous simulations. However, no systematic uncertainty budget was included in their analysis.

To optimally account for this contamination, Kunz et al. (2007) developed the Bayesian Estimation Applied to Multiple Species (BEAMS) method to independently model the SNe Ia and CC Hubble residual distributions. BEAMS samples both Ia and CC species of SNe and simultaneously fits for the contribution of each while marginalizing over nuisance parameters. BEAMS relies on a classifier, such as the aforementioned PSNID or SuperNNova, to assign SNe Ia probabilities and bifurcate the distribution into likely Ia and CC. The first cosmological measurement using BEAMS was done by Hlozek et al. (2012) on the Sloan Digital Sky Survey (SDSS) sample, but did not include a systematic uncertainty

budget. The systematic uncertainties were considered by Knights et al. (2013), which developed a BEAMS formalism that gives reliable estimations of cosmological parameters. Jones et al. (2018a) used their own implementation of BEAMS and were the first to evaluate the systematic uncertainty budget for a photometric sample (the PS1 sample).

BEAMS was further improved by Kessler & Scolnic (2017), incorporating bias corrections and the option of using a simulated CC sample instead of ad-hoc fit parameters to describe the CC Hubble residuals. This method, known as BEAMS with Bias Corrections (BBC), was first applied to a real photometric sample in Jones et al. (2018b). The bias correction component was included in S18 for their spectroscopic sample and also the DES 3 yr sample (Brout et al. 2018; Abbott et al. 2019).

Analyzing a sample with contamination relies on accurate models of CC SNe to simulate training samples for classifiers and validation. Previous analyses have used spectroscopically confirmed light curves of non-Ia SN to develop rest-frame Spectral Energy Distribution (SED) templates for simulations, in order to generate CC events at all redshifts. The first collection of non-Ia SED templates came from Kessler et al. (2010b), which released a simulated sample of mixed SNe Ia and non-Ia light curves for a classification challenge—SN Photometric Classification Challenge (SNPHOTCC). Most recently, the Photometric LSST Astronomical Time-series Classification Challenge (PLAsTiCC; The PLAsTiCC team et al. 2018) has gathered a large library of new SED templates (Kessler et al. 2019) that can be used for simulating training samples, further expounding upon previous efforts. The SED templates included in this release span a wider variety of transient events than those in SNPHOTCC. The PLAsTiCC SED templates have not yet been used to simulate training samples as part of the analysis of a real photometric sample; here we make the first attempt.

Current cosmological analyses with photometric samples use spectroscopically confirmed host-galaxy redshifts to create a Hubble diagram. A systematic method of identifying host galaxies was introduced in Sullivan et al. (2011) with the concept of directional light radius (DLR), which uses galaxy orientation and spatial size to determine the most likely host galaxy for each SN. This DLR method was further explored in Gupta et al. (2016) and Sako et al. (2018). Gupta et al. (2016) include other properties in the host assignment, and evaluate the frequency of misassociation of the host galaxies. This systematic uncertainty was evaluated in Jones et al. (2018b), and is evaluated here with an improved technique. The spectroscopic targeting of galaxies based on their brightness should cause an additional systematic bias in the cosmological measurements because host-galaxy properties have been found to be correlated with SN luminosity (Sullivan et al. 2011); we assess the impact of this bias.

To examine the impact of CC modeling in simulated training sets for classifiers, as well as host-galaxy selection, we perform a reanalysis of the SDSS-II SN Survey (Frieman et al. 2008). Here, we use models from PLAsTiCC for the simulated training sample and the BBC method to construct our Hubble diagram. This paper is the first of two works. In this work, we evaluate systematic uncertainties in the photometric analysis of the SDSS sample that would not be included in a conventional spectroscopic analysis, e.g., S18. This paper also includes a broader range of CC models using PLAsTiCC, and improved methods for evaluating systematic uncertainties arising from misassociated hosts. SDSS is the only publicly available photometric sample without previously applied selection cuts. Therefore, the methods presented here can be checked and improved by the community.

In the next paper, we will measure nuisance and cosmological parameters from this sample and compare to those from the Pan-STARRS photometric sample. We will also combine these two photometric samples for a cosmological measurement.

The layout of this paper is as follows. A review of the data is presented in Section 2. Our analysis techniques and assignment of host galaxies are detailed in Section 3. The simulations for bias corrections and training samples are described in Section 4. An evaluation of different systematic uncertainties is explored in Section 5. Finally, Section 6 contains our conclusions

2. Data Sample

The SDSS began in 2000 as the first wide-area sky survey using charge-coupled devices (York et al. 2000). A review of the SDSS SN Survey is given in Frieman et al. (2008). In brief, Stripe 82 (from R.A. of 20^{h}–04^{h} and $2.^{\circ}5$ wide along the equator in decl.) was repeatedly scanned every four days using *ugriz* filters. The processing pipeline for the images is described in Stoughton et al. (2002) and potential SNe were identified in subtracted images with the method developed by Alard & Lupton (1998). Candidate selection and spectroscopic identification are described by Sako et al. (2008). The photometry is described in Holtzman et al. (2008). The spectroscopically confirmed subset of this data was used in several analyses to measure cosmological parameters (Kessler et al. 2009a; Betoule et al. 2014; Scolnic et al. 2018).

Through three observing seasons (Fall 2005 through Fall 2007), the SDSS SN program discovered 10,258 new variable objects (Sako et al. 2018) and measured their *ugriz* light curves. Further specifics of the SNe population statistics can be found within Sako et al. (2018). A component of the SDSS SN survey included spectroscopic follow-up for a limited number of identified host galaxies.

A separate SDSS spectroscopic survey (the Baryon Oscillation Spectroscopic Survey, or BOSS) acquired a significant fraction of potential host-galaxy redshifts (Dawson et al. 2013). For 4680 candidates, they obtained accurate spectroscopic redshifts of the corresponding host galaxies. Since the conclusion of the SDSS SN Survey in 2008, BOSS has acquired an additional 1294 host-galaxy spectroscopic redshifts. Figure 1 shows the spectroscopic redshift (spec-z) and photometric redshift (photo-z) distributions for SDSS and BOSS.

The data release from Sako et al. (2018) has galaxies assigned using the position of the SNe from the first SN detection epoch, which typically has a low signal-to-noise ratio (S/N); here we reassign the host galaxies using the averaged position of the SNe from all detections. This change in coordinate calculation is minor—the mean difference in angular separation values is $0.''1$, with a standard deviation of $1.''4$.

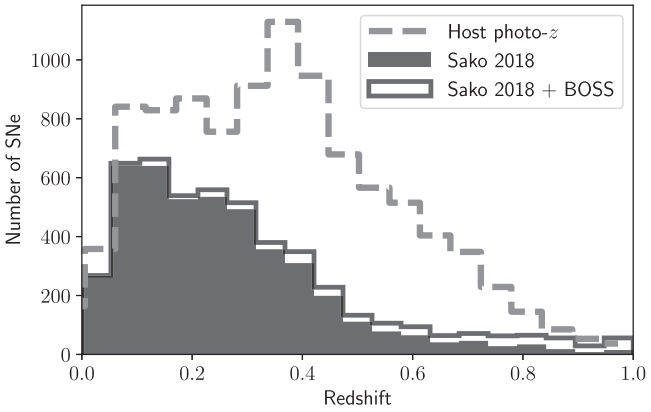

Figure 1. Redshift distribution of the SDSS transient sample. In the filled histogram we show the distribution of spec-z of the host galaxies from Sako et al. (2018); in the solid histogram we show the distribution including the 1294 host-galaxy spec-z from BOSS. The dashed histogram is the host-galaxy photo-z distribution found for all SDSS transients.

3. Analysis

Measuring cosmological parameters with SNe Ia requires modeling and fitting the observed light curves and using the results to standardize SN brightness for distance measurements. Distances are evaluated with the Tripp equation, detailed in Equation (4) in Abbott et al. (2019) and Equation 3 in S18. Simulations are also needed to correct for distance biases and to generate training samples for classifiers. We review the main steps of the analysis here.

To better understand our systematic uncertainties, we simulated 30,000 events and split them into 40 data-sized samples so that each simulated subsample is comparable in size to our real data sample (∼700 SNe). The full analysis is performed on each simulated subsample as well as the true data sample.

3.1. Host Matching

To match a SN to its most likely host galaxy, the $d_{\rm DLR}$ method is employed. This uses angular separation ($\Delta\theta$) and accounts for the galaxy spatial profile and orientation. The derivation for $d_{\rm DLR}$ is shown in the appendix. Gupta (2013) also provides a detailed derivation.

For each SN, all galaxies within 30″ are selected and sorted by ascending $d_{\rm DLR}$ values. The galaxy with the smallest $d_{\rm DLR}$ is considered to the host galaxy.

3.2. Light-curve Fitting

SN light-curve fits are done with the SALT2 light-curve model (Guy et al. 2010, hereafter G10) using the improved model from the Joint Light-curve Analysis (Betoule et al. 2014). The light-curve fitting and selection requirements are implemented with the SuperNova Analysis (SNANA) software package (Kessler et al. 2009b).

Selection requirements (cuts) are applied to reduce CC contamination and to define a sample that has distance biases that can be modeled with a Monte Carlo simulation. SNe with properties within the SALT2 training range of color ($-0.3 < c < 0.3$) and stretch ($-3 < x_1 < 3$) are selected. To ensure well-measured light-curve fit parameters, we apply cuts on the uncertainties for stretch ($\sigma_{x_1} < 1$) and time of maximum brightness ($\sigma_{t_0} < 2$ observer frame days). We also require that the SALT2 fit probability (based on χ^2 per degree of freedom) be >0.001. Next, we define a rest-frame age, $T_{\rm rest} = ({\rm MJD} - {\rm MJD}_{\rm peak})/(1+z)$, where MJD is the observation date, $\rm MJD_{peak}$ is the date of peak brightness, and z is the redshift. We require that at least one observation satisfies $T_{\rm rest} > 10$ days, and that at least one observation satisfies $T_{\rm rest} < 0$ days. Finally, we require that at least two bands have an epoch in which the S/N is >5. A summary of these cuts on the data are is in Table 1.

Table 1
Sequential Selection Requirements on the SDSS Transient Sample

Cut	Number	Comments
Total Candidates	10,258	Data Release (Sako et al. 2018)
Spec-z and $d_{\rm DLR}$	4356	Host galaxy redshift
$T_{\rm rest} < 0$	3852	Light-curve sampling
$T_{\rm rest} > 10$	3518	Light-curve sampling
S/N	2717	Signal-to-Noise Ratio > 5
SALT2 Fit Parameters	1219	c, x_1, σ_{x1}, σ_{t0}
NN Classifier	700	Nearest Neighbour classifier

3.3. Classification

We use a Nearest Neighbour (NN) classifier developed by Sako et al. (2018) and Kessler & Scolnic (2017). We simulate a large training sample of SN (Ia + CC) with the same selection requirements and light-curve fitting as for the data. The redshift, color, and stretch (z, c, and x_1) are used to define a three-dimensional space for the NN analysis. In this space, each data point (real or simulated) is the center of a sphere at $\{z, c, x_1\}$. Classification is done by counting the number of Ia and CC SN within the sphere, and the data point is classified to be the type that is most frequent inside the sphere. The size of the sphere is set with a metric determined by maximizing the product of the efficiency and purity (Kessler & Scolnic 2017). Data identified as SNe Ia with a probability of less than 0.5 are rejected.

3.4. BBC and Cosmology Fitting

Cosmological analysis within the BBC framework is done in three stages. The first stage classifies SNe as Ia or CC using the NN method, and assigns a probability ($P_{\rm Ia}$) for each event to be a SNe Ia. The second stage separates the data into redshift bins and determines a mean distance modulus in each bin, after accounting for selection biases and CC contamination (Kessler & Scolnic 2017). Here we use 10 equal sized bins ranging from $z = 0.02$ to 0.5. The third stage performs a cosmological fit to the binned distances using BAO (Eisenstein et al. 2005) and CMB (Komatsu et al. 2009) priors, similar to Lasker et al. (2019) who found these priors to be sufficient for systematics studies.

4. Simulations

Simulated SNe are needed to calculate bias corrections, create training samples, and assess the impact of our systematics. We use the SNANA software to simulate SN light curves using SDSS detection efficiencies, point-spread function sizes, sky noise, and zero-points. The observing history has previously been modeled for SDSS in Kessler et al. (2009b). While Kessler et al. (2009b) modeled the spectroscopic selection efficiency of the SNe, here we model the

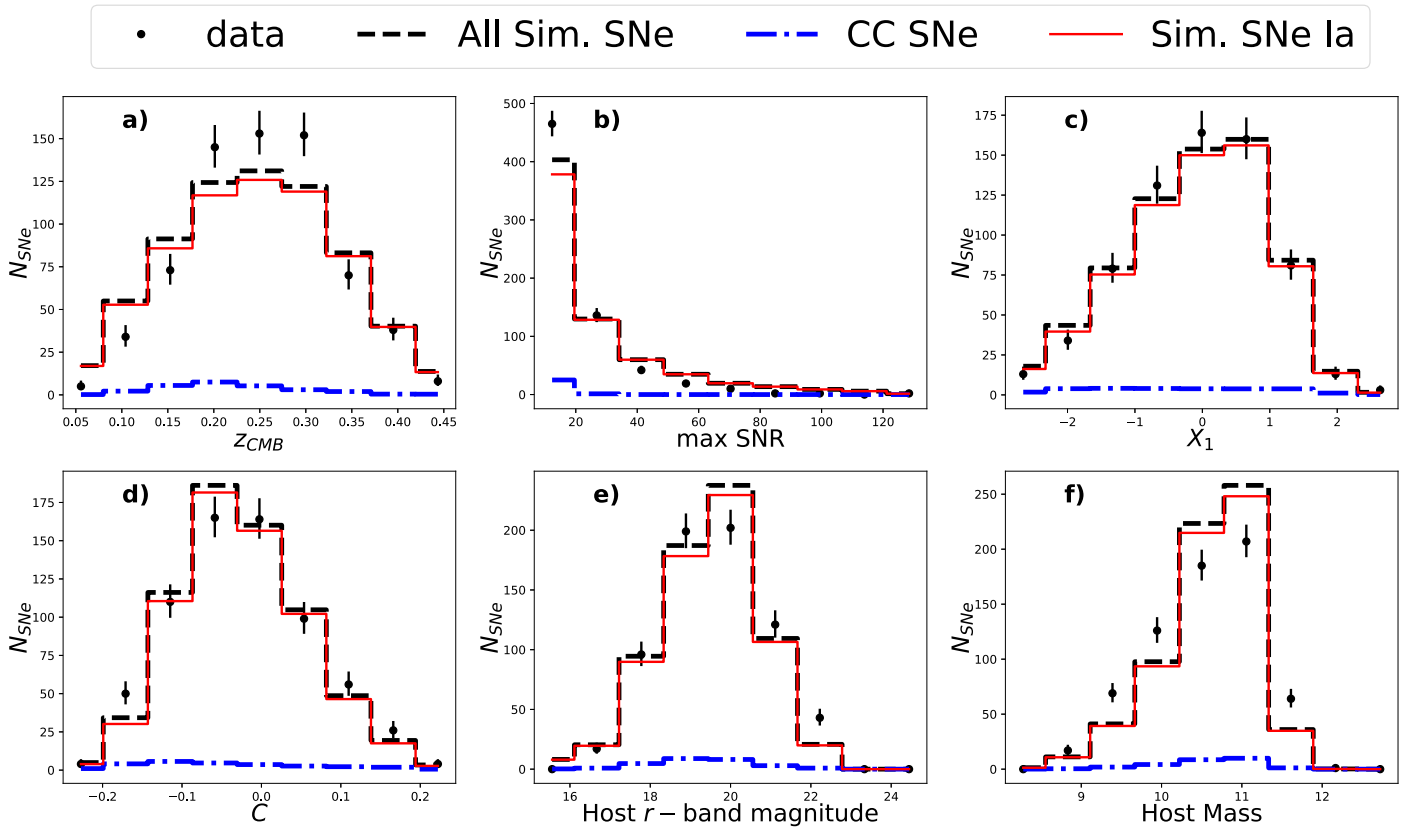

Figure 2. Comparison between the data and the Fiduciary simulation for various distributions. The data are shown in points with error bars, the dashed histogram shows the total simulated SNe (Ia + CC), the solid histogram shows the simulated SNe Ia only, and the dotted histogram shows simulated CC. The simulated CC contamination is ∼4% of the total sample and is discussed further in Section 5.

efficiency of obtaining a spectroscopic redshift from the host galaxy, as described below. A complete description of how these simulations are generated for DES is given in Kessler et al. (2019); for this study we replace the survey description of DES with that for SDSS. We simulate our SNe with ΛCDM cosmology, with a flat universe ($k = 0$), $\Omega_{\rm Matter} = 0.3$ and $w = -1$.

For this analysis, we simulate both Type Ia and CC light curves. For SNe Ia, we use the SALT2 model with population parameters from Scolnic & Kessler (2016). Simulations were generated with the stretch luminosity α and color luminosity β that were measured from the data as input ($\alpha = 0.14$ and $\beta = 3.2$; Sako et al. 2018). We use the "G10" intrinsic scatter model from Kessler et al. (2013) using the error parameterization from Guy et al. (2010). CC modeling is done with SED templates from Kessler et al. (2010b), Jones et al. (2018a), and the PLAsTiCC templates from Kessler et al. (2019), further detailed in Section 5.1. We denote our "Fiduciary" analysis using PLAsTiCC CC templates (excluding SNIax) in the training sample along with an adjusted luminosity function to match Jones et al. (2018b). Figure 2 shows the distributions of data are in good agreement with those from the Fiduciary simulations for redshift, S/N, color, and stretch.

4.1. Host Galaxy Libraries and Comparison of Distributions between Data and Simulations

To model the potential measurement biases of cosmological parameters based on selection of host galaxies, we first create a realistic library of host galaxies (HOSTLIB) with properties that match those of our data. We evaluate the quality of our HOSTLIB by comparing the distributions of the smallest and second smallest $d_{\rm DLR}$ (Section 3.1); these distributions are sensitive to galaxy spatial profile, survey depth, galaxy photo-z, and $\Delta\theta$.

We evaluated three different HOSTLIBs to use in our simulations. The first two, the Advanced Camera for Surveys General Catalog (ACS-GC), and the Marenostrum Institut de Ciències de l'Espai Simulations Catalogue, were used in Gupta et al. (2016). For these two HOSTLIBs, the simulated $\Delta\theta$ distribution does not match the SDSS data.

Therefore, we created a third library by compiling observed galaxies within Stripe 82 from the SDSS DR14 data release. To maximize completeness and exclude spectroscopic selection effects, we selected host galaxies with a photometric redshift. The HOSTLIB includes Sérsic profile information calculated from the Stokes values. These profiles are used in simulations to place SNe near a galaxy and to model Poisson noise from the host galaxy. The SNANA simulation only calculates the smallest $d_{\rm DLR}$ value for each SN, so the second smallest values were calculated separately from the HOSTLIB.

For data and simulation, Figure 3 compares distributions of $\Delta\theta$, DLR, and $d_{\rm DLR}$. Each distribution is shown separately for the smallest and second smallest $d_{\rm DLR}$ value. Also shown is the ratio of the smallest to second smallest $d_{\rm DLR}$ values ($r_{\rm DLR}$). We find good agreement in all distributions. Note that a HOSTLIB with too-large separations between galaxies can result in good data/sim agreement for the smallest $d_{\rm DLR}$ in Figures 3(a)–(c), but would result in poor agreement for the second smallest

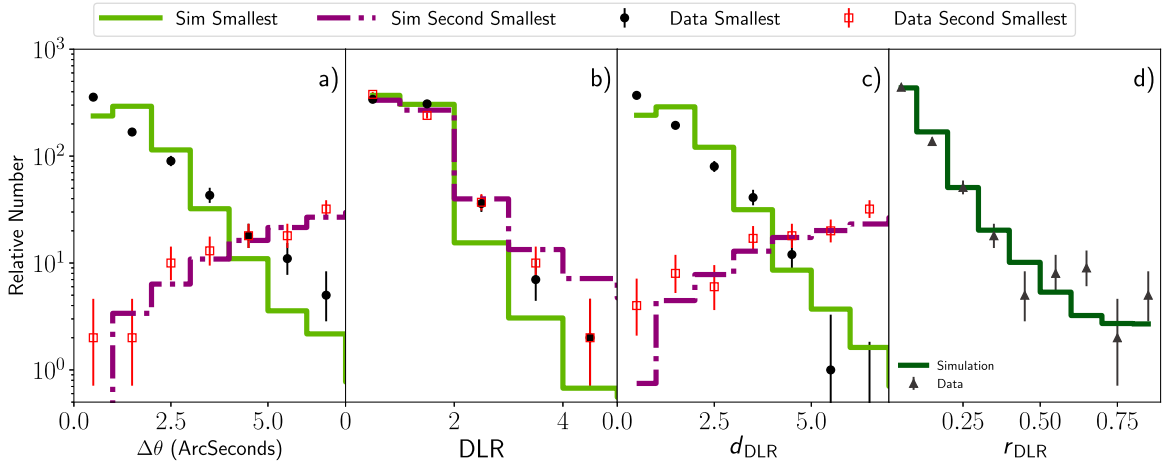

Figure 3. Distributions for data (filled circles and open squares) and the Fiduciary SNe Ia-only simulation (histogram) for quantity are indicated in each panel, as defined in Section 3.1. For panels (a), (b), and (c) the filled circles and solid histogram are for the smallest d_{DLR} value; the open squares and dashed histogram are for the second smallest value. In (d), r_{DLR} is shown by triangles for data and a solid histogram for the simulation.

d_{DLR}, and also underpredict misassociations. The good agreement for the second smallest d_{DLR} and r_{DLR} is therefore an important metric for reliably predicting the misassociation rate. We also show in Figure 2(e) that there is good agreement in the r-band magnitude of the host-galaxy distribution between data and simulations.

Past studies have shown that there is a correlation between the stretch-and-color-corrected luminosity of SNe Ia and the host-galaxy stellar mass ($M_{stellar}$). This effect has been found in the SN Legacy Survey (Sullivan et al. 2010), the SDSS sample (Lampeitl et al. 2010; Gupta et al. 2011b; Hayden et al. 2013; Wolf et al. 2016), and the PS1 sample (S18). In this SDSS analysis, we simulate these correlations to estimate biases arising from our spectroscopic galaxy selection. For every galaxy in our HOSTLIB, we calculate $M_{stellar}$ using the methodology from Taylor et al. (2011),

$$M_{stellar} = 1.15 + 0.7 \times (g - i - 0.4 \times (i - \mu_{calc})), \quad (1)$$

where g and i are the host-galaxy magnitudes in the respective band, and μ_{calc} is the calculated distance modulus using the galaxy redshift and the same ΛCDM cosmology parameters as in the simulations. Equation (1) is used to calculate masses for both the data and the HOSTLIB. A comparison of the host-mass distribution between data and simulations is shown in Figure 2(f); while the agreement is not as good as that for the host-galaxy magnitude comparison and could use further study, it is sufficient to assess systematics.

We introduce a -0.025 mag correction to the luminosity of SNe in galaxies with stellar mass $M_{\odot} > 10^{10}$, and a $+0.025$ mag correction to those with $M_{\odot} < 10^{10}$. We do not include additional correlations of SNe Ia properties (c and x_1) with host-galaxy properties; these correlations are discussed in Smith et al. (2014).

Using simulations generated with input from our HOSTLIB, we evaluate the selection efficiency of our host galaxy. In our Fiduciary analysis, we define the efficiency, $\epsilon_{host}(r)$, to be a function of host-galaxy r-band magnitude as follows:

$$\epsilon_{host}(r) \equiv N_{data}(r)/N_{sim}(r), \quad (2)$$

where $N_{data}(r)$ is the number of SNe in each host-galaxy r-band magnitude bin for data, and $N_{sim}(r)$ is the number of SNe in each host-galaxy r-band magnitude bin for a simulation with

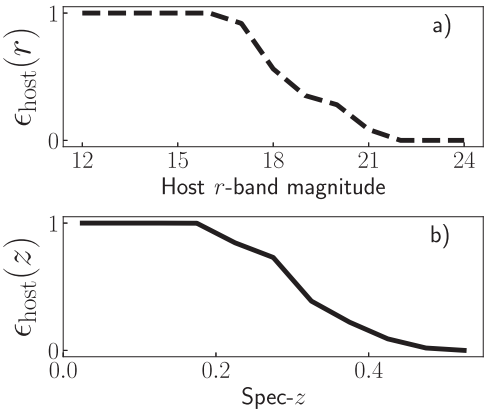

Figure 4. Measured r-band host magnitude efficiency is shown as the black dashed line and the measured host spec-z efficiency is shown as the solid black line. The spec-z efficiency is roughly half at $z = 0.3$. The r-band host magnitude efficiency drops off at the faint end.

$\epsilon_{host}(r) = 1$. We scale $\epsilon_{host}(r)$ so that the maximum is 1 (Figure 4(a)).

For a systematic test, we follow Jones et al. (2018b) and parameterize the selection function to depend on host spec-z (Figure 4(b)):

$$\epsilon_{host}(z) \equiv N_{data}(z)/N_{sim}(z), \quad (3)$$

where z is the host-galaxy spec-z, and $N_{data}(z)$ and $N_{sim}(z)$ are defined as in Equation (2), but using z bins.

4.2. CC Simulations

An important systematic in cosmological analyses of photometric samples is the collection of CC models used to simulate training samples for classifiers. The most recent study on this systematic was done by Jones et al. (2018b), which used a compendium of publicly available CC templates and adjusted the luminosity functions of the library to match the Hubble residual tail region after selection cuts. Light-curve templates of SNII were adjusted by 1.1 mag to be more luminous and SNIb/c were similarly adjusted by 1.2 mag.

Since Jones et al. (2018b), the PLAsTiCC library (Kessler et al. 2019) was released, which has enhanced previous CC template libraries. Compared with Jones et al. (2018b), here we

Table 2
w Differences for Systematic Tests

Systematic Test (Host)	$\Delta w_{\rm sim}$ [a]	$w_{\rm rms}$ [b]	$\Delta w_{\rm data}$ [c]	N_σ [d]
Misassociated Host	+0.0007(09)	0.0059	N/A	N/A
Host Efficiency	−0.0072(37)	0.0237	−0.006	0.05σ
Systematic Test (Contamination)	$\Delta w_{\rm sim}$	$w_{\rm rms}$	$\Delta w_{\rm data}$	N_σ
No LF adjustment	−0.0109(03)	0.0192	−0.041	1.57σ
Choice of CC model	−0.0028(14)	0.0089	−0.002	0.09σ
Include Iax	−0.0022(09)	0.0059	+0.001	2.07σ

Notes.
[a] Mean Δw of the 40 simulated subsamples.
[b] The rms of the simulated subsamples.
[c] The Δw measured by the data.
[d] The number of standard deviations of Δw for data away from Δw for sim, defined in Equation (6).

include MOSFiT (Modular Open-Source Fitter for Transients) for SNIbc (Kessler et al. 2010a; Villar et al. 2017; Guillochon et al. 2018; Pierel et al. 2018), Nonnegative Matrix Factorization (NMF) for SNII (Kessler et al. 2010a; Villar et al. 2017; Guillochon et al. 2018; Pierel et al. 2018), SNIax (Jha 2017), and SNe Ia-91bg. We included an additional 0.9 mag smear for SNII-NMF as discussed in Kessler et al. (2019). Our Fiduciary analysis includes SNII-NMF, SNIbc-MOSFiT, and SNe Ia-91bg. As we will discuss in the next section, SNIax were excluded from both the simulated training and data samples.

4.3. SNIax Simulations

The PLAsTiCC models include SNIax, which typically have lower luminosity, lower ejecta velocity, and greater variation in photometric parameters than their SNe Ia counterparts. The SED model used in PLAsTiCC is based on the real SNIax, 2005hk. The SED model was augmented with other spectra and the luminosity function was inferred from the sample studied in Jha (2017). Light curves are generated to match the absolute magnitude (M_V), rise time ($t_{\rm rise}$), and decline rate in the B and R bands ($\Delta\ m_{15}(B)$ and $\Delta m_{15}(R)$) detailed in Stritzinger et al. (2015) and Magee et al. (2016c).

4.4. Simulation Analysis

We apply the analysis (Section 3) to our simulated data sample, and fit for nuisance parameters α, β, γ, and cosmological parameter w. The recovered values for these parameters in our Fiduciary analysis are consistent with their input values of 0.14, 3.2, 0.05, and −1, respectively. More precise validation tests with simulations are described in Section 6 of Brout et al. (2018).

5. Results

Here we assess the impact on our cosmological measurements of the systematics studied in this analysis, such as different CC templates used in classifier training sets, the frequency of host-galaxy misassociation, and the modeling of selection efficiency. A summary of the various cosmological biases from these uncertainties is presented in Table 2. The mean bias in w is determined with the 40 simulated subsamples

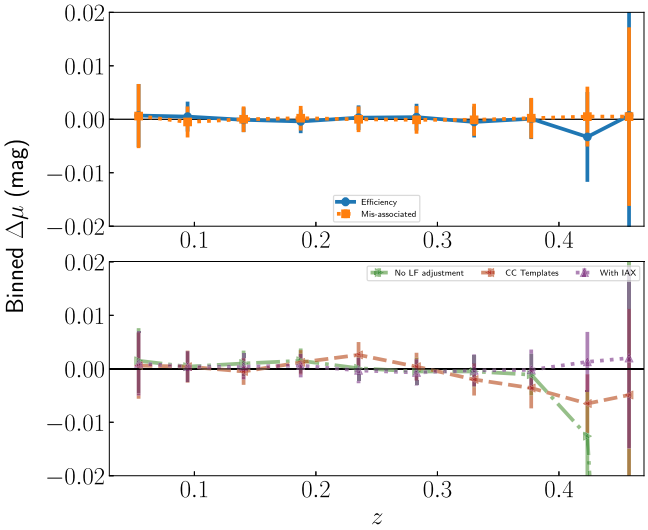

Figure 5. Difference between binned distance modulus residuals for each systematic are shown here, for simulated supernovae. The top panel shows the effect of host-galaxy selection changes, and the bottom panel shows the different CC options.

for each systematic listed in Table 2, which has previously been discussed individually. In addition, the error on the mean and the scatter, or robust standard deviation, have also been calculated for the simulations. We define

$$\Delta w \equiv w_{\rm Fid} - w_{\rm sys} \tag{4}$$

as the w-bias. For data, $w_{\rm Fid}$ is the measured w value for the Fiduciary analysis. For simulations, $w_{\rm Fid}$ is the mean measured w of our subsamples. The bias in recovered distances as a function of redshift due to each systematic uncertainty is shown in Figure 5. We define the statistical error ($w_{\rm stat}$) as

$$w_{\rm stat} = w_{\rm rms}/\sqrt{N_{\rm sub}}, \tag{5}$$

where $w_{\rm rms}$ is the rms of Δw and $N_{\rm sub}$ is the number of subsamples. With 40 subsamples, the statistical error in our mean Δw is below 0.004, which is sufficiently small for this analysis.

Host galaxy misassociation and shifts in the CC luminosity function result in a w-bias that can be corrected, and the resulting systematic uncertainty is typically smaller than the correction. Here we use the size of each correction as a systematic uncertainty, and in future work will evaluate the reliability of these corrections along with the associated systematic uncertainties.

5.1. Galaxy Association and Misassociation

Figure 3 shows the properties used to validate the simulations from which the misassociation rate was determined. Comparing each true host galaxy in our simulation to the $d_{\rm DLR}$-selected galaxy, we determine the host-galaxy misassociation to be 0.6%.

Figure 6 shows the effect of misassociated hosts on redshifts (Figure 6(a)), as well as the distributions of $\Delta\theta$ (Figure 6(b)) and $d_{\rm DLR}$ (Figure 6(c)) for those misassociated hosts; Figure 6(d) is a histogram of $r_{\rm DLR}$ for misassociated SN. In each panel, the distribution for misassociated hosts is much broader compared to correctly identified hosts.

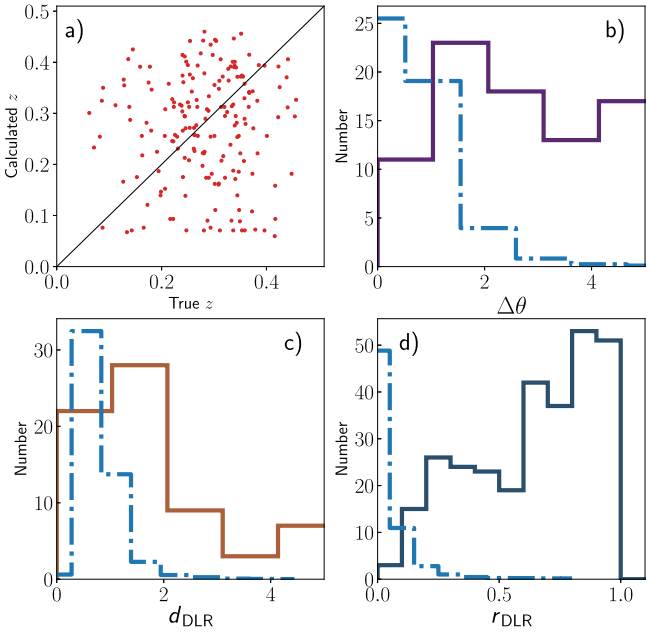

Figure 6. For simulated supernovae with misassociated hosts, panel (a) shows true values of redshift vs. the calculated values, with the black line showing correct associations for reference. The solid histograms in panels (b)–(d) show distributions only for the misassociated supernovae, and the dashed–dotted histogram represents all supernovae (normalized to the misassociated population). When the galaxy is misassociated, we attribute SNe to higher-redshift hosts 56% of the time and lower-redshift hosts 44% of the time.

We find that the recovery of w is biased by $\Delta w = 0.0007$ by this misassociation, which is consistent with 0.

5.2. Impact of Host Galaxy Selection Efficiency

We evaluate the bias on w due to our host-galaxy selection by comparing our recovered distances using $\epsilon_{\rm host}(r)$ to those using $\epsilon_{\rm host}(z)$. The impact on the binned distances is shown in Figure 5. For most of the redshift range, the impact is less than 2 milli-mags and the only significant impact is at the higher end of our redshift range. This produces a w-bias of $\Delta w = -0.0072 \pm 0.0037$, significantly smaller than the statistical uncertainty. The rms around this value is 0.05σ.

5.3. Impact of CC Templates

Figure 7 shows the Hubble residual distributions using five different CC models in the analysis, and each model is indicated in the panel. Figure 7 contains our Fiduciary case, where CC templates used in the simulations are from the PLAsTiCC models with an adjusted luminosity function and without SNIax; the PLAsTiCC model with neither adjusted luminosity function nor SNIax; the PLAsTiCC model with adjusted luminosity function and SNIax; the CC templates from Kessler et al. (2010b) without luminosity adjustments (K10); and the CC templates from Jones et al. (2018a) with adjustments. The smallest contamination ($P_{\rm CC}$) is 1% for K10, and the highest is 5.9% for the Fiduciary with Iax analysis. Still, we see that the contamination in the data for the positive tail of the Hubble residual distribution is better predicted in some cases than others. We find that the PLAsTiCC and K10 models do not match the data well in this region, confirming the need for luminosity function corrections to match the high Hubble residual tail suggested in Jones et al. (2018a).

For the case of Fiduciary with SNIax, the SNIax make up 40% of the CC contamination. While the SNIax luminosity distribution is fainter than that of SNe Ia, we also find that the x_1 and c values satisfy the selection requirements (see Section 2), and therefore the NN classification poorly separates SNe Ia from SNIax. Jones et al. (2018b) do not include SNIax in the contamination library due to the expectation that they are too red ($c > 0.3$), and because the SNIax model was not available. As discussed in Section 4.3, only a single SN was used to generate the SNIax model. However, if we perform SALT2 light-curve fits on the four known SNIax in SDSS (including 2005hk), we find that all the SNIax have fitted color values $c > 0.3$ and thus fail our selection requirements. Therefore, these light-curve fits suggest that the SNIax contamination is overestimated and further study is needed.

From simulations, the impact on w due to the systematics related to CC libraries is given in Table 2. We find the mean bias due to the CC systematics is $\Delta w < |0.01|$, with a statistical uncertainty of $\sim$0.001. The rms in w from the simulations due to the systematics is 0.01–0.02.

5.4. Data and Simulation Comparison

In the last two columns of Table 2, we show the impact on w of the systematics studied in this analysis for the real data sample. This is shown for all the systematics except for the misassociated host, as there we cannot apply the same technique on the data as we did for the simulations. To assess whether the changes seen for the data sample are consistent with predictions from the simulations, we define the number of standard deviations (N_σ) for each systematic as

$$N_\sigma = (\Delta w_{\rm sim} - \Delta w_{\rm data})/w_{\rm rms}, \quad (6)$$

where $\Delta w_{\rm sim}$ is the Δw recovered in simulations, $\Delta w_{\rm data}$ is the Δw recovered from the data, and $w_{\rm rms}$ is the rms of the Δw recovered from simulations. We find that the highest deviation compared to the simulations is seen for the "No LF adjustment" systematic at 2.1σ. All other deviations near or below $<1\sigma$. Therefore, we conclude that the impacts of the systematics seen in the simulations are consistent with those seen for the data.

6. Discussion and Conclusions

In this paper, we have presented new methodologies for two systematic uncertainty contributions unique to analyses of cosmology with photometric SNe Ia samples: (1) host-galaxy misassociation and selection efficiency, and (2) CC training library. For classifier training and bias corrections, we generated realistic simulations of SN (SNe Ia and CC) and host galaxies. We validated these simulations with a wide range of diagnostics. We find the host-galaxy misassociation rate to be 0.6%, resulting in a w-bias of $\Delta w = 0.0007$. We expect the misassociation rate, and hence the distribution of misassociated redshifts, to change with the redshift range of a survey. If the impact of this systematic increases in future analyses, more rigorous bias correction simulations and possibly new analysis methods such as z-BEAMS (Roberts et al. 2017) may be necessary.

The galaxy selection efficiency contributes a w-bias of $\Delta w = -0.0072 \pm 0.0037$. For the first time, the PLAsTiCC library has been used for assessing systematic uncertainties in a cosmological analysis. We confirm the Jones et al. (2018a) finding that CC luminosity function adjustments are needed to

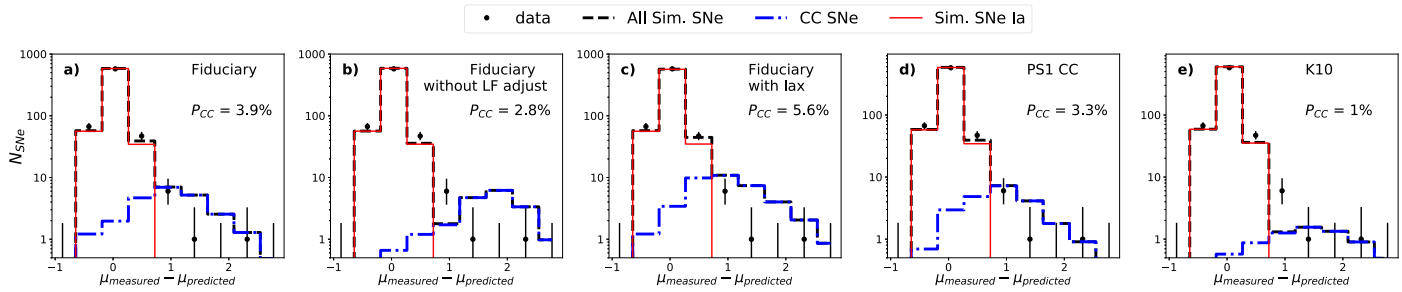

Figure 7. Hubble residual distribution for data, and for simulations using different CC models as indicated on each panel. $\mu_{\rm measured}$ is the measured Tripp distance modulus and $\mu_{\rm predicted}$ is the predicted distance modulus from ΛCDM cosmology. The training sample is the Fiduciary CC model in all cases. Data are shown with points, simulated SNe Ia are shown with a red histogram, and simulated CC SNe are shown with a blue dashed histogram. The combined simulated distribution of CC and Ia SNe is shown with a black dashed histogram. The non-SNe Ia contamination ($P_{\rm CC}$) is shown for each panel.

more accurately predict the Hubble residual tail (see Figure 7). We find that ignoring the CC luminosity function shift results in a w-bias of $\Delta w = -0.0109 \pm 0.0003$.

The scale of these systematics is similar to that found in Jones et al. (2018a), given similar priors, for the contamination systematics, though they do not explicitly include systematics for galaxy misassociation or the efficiency of host-galaxy follow-up. The systematic shifts in the data are well predicted by the simulations, as shown in Table 2.

The total statistical uncertainty on w from a cosmological fit to the SDSS sample with the same priors as discussed in Section 4 is 0.1, larger than the systematics investigated here. For larger samples, the statistical uncertainty will be smaller and systematic uncertainties of this size will be more significant. Here we have developed a framework that can be used to evaluate these systematic uncertainties in future analyses of photometric samples.

Appendix

A.1. Discussion of $\rm d_{DLR}$ Values

We start with the radial equation of an ellipse as measured from the center, with semimajor and semiminor axes a and b and orientation angle θ:

$$r(\theta) = \frac{ab}{\sqrt{(a\sin\theta)^2 + (b\cos\theta)^2}}. \quad (7)$$

We define the SN angle as the angular difference between a line that goes through the SN position and galaxy center and a line that passes through north and the galaxy center. Combined with the orientation of the galaxy as given by the galaxy position angle we define θ by subtracting the SN angle from the position angle of the galaxy. With a, b, and θ, the DLR is defined from Equation (7) as the effective radius of the galaxy at angle θ.

The position angle of the galaxy can be found using the Stokes parameters Q and U given in the SDSS DR14 data release. DR14 uses a slightly unconventional notation for U; this is corrected with a factor of 2 in the position angle.

Since these parameters are not fits to a model, but rather based on pixel data, they are more robust for fainter galaxies. The position angle ϕ can be expressed as

$$\phi = \frac{1}{2}\arctan\left(\frac{2U}{Q}\right). \quad (8)$$

The ratio of the semimajor and minor axes can also be computed with the Stokes parameters. Defining $\kappa \equiv Q^2 + U^2$, the ratio a/b is then expressed as

$$\frac{a}{b} = \frac{1 + \kappa + 2\sqrt{\kappa}}{1 - \kappa}. \quad (9)$$

Following Sako et al. (2018), we set a equal to the Petrosian half-light radius within the r-band and b is determined using Equation (9). Finally, we define a distance-weighted $d_{\rm DLR}$ as

$$d_{\rm DLR} = \frac{\text{Angular separation}}{r(\theta)}. \quad (10)$$

It is important to note that DLR and $d_{\rm DLR}$ are survey-dependent quantities and are not easily comparable across surveys. Of particular note are magnitude cutoffs. Establishing a magnitude limit does allow for fine-tuned control of $\Delta\theta$ density, but does not account for apparent ellipticity. At higher magnitudes, the apparent ellipticity as measured by the Stokes parameters begins to increase. At fainter brightness, noise begins to dominate the signal and leads to unrealistic ellipticity measurements. But differences in magnitude limits for different surveys, combined with those in image processing, can alter the apparent size of a galaxy. Self-consistent DLR measurements within the survey are more accurate than solely $\Delta\theta$ determinations, but cross comparison would not be effective.

ORCID iDs

Dan Scolnic https://orcid.org/0000-0002-4934-5849
Richard Kessler https://orcid.org/0000-0003-3221-0419

References

Abbott, T. M. C., Allam, S., Andersen, P., et al. 2019, ApJL, 872, L30
Alard, C., & Lupton, R. H. 1998, ApJ, 503, 325
Anderson, L., Aubourg, É., Bailey, S., et al. 2014, MNRAS, 441, 24
Bennett, C. L., Halpern, M., Hinshaw, G., et al. 2003, ApJS, 148, 1
Bernstein, J. P., Kessler, R., Kuhlmann, S., et al. 2012, ApJ, 753, 152
Betoule, M., Kessler, R., Guy, J., et al. 2014, A&A, 568, A22
Brout, D., Scolnic, D., Kessler, R., et al. 2018, arXiv:1811.02377
Campbell, H., D'Andrea, C. B., Nichol, R. C., et al. 2013, ApJ, 763, 88
Conley, A., Guy, J., Sullivan, M., et al. 2011, ApJS, 192, 1
Dawson, K. S., Schlegel, D. J., Ahn, C. P., et al. 2013, AJ, 145, 10
Eisenstein, D. J., Zehavi, I., Hogg, D. W., et al. 2005, ApJ, 633, 560
Frieman, J. A., Bassett, B., Becker, A., et al. 2008, AJ, 135, 338
Guillochon, J., Nicholl, M., Villar, V. A., et al. 2018, ApJS, 236, 6
Gupta, R. R. 2013, PhD thesis, Univ. Pennsylvania
Gupta, R. R., D'Andrea, C. B., Sako, M., et al. 2011b, ApJ, 740, 92
Gupta, R. R., Kuhlmann, S., Kovacs, E., et al. 2016, AJ, 152, 154
Guy, J., Sullivan, M., Conley, A., et al. 2010, A&A, 523, A7

Hayden, B. T., Gupta, R. R., Garnavich, P. M., et al. 2013, ApJ, 764, 191
Hlozek, R., Kunz, M., Bassett, B., et al. 2012, ApJ, 752, 79
Holtzman, J. A., Marriner, J., Kessler, R., et al. 2008, AJ, 136, 2306
Ivezić, Ž., Kahn, S. M., Tyson, J. A., et al. 2019, ApJ, 873, 111
Jha, S. W. 2017, in Handbook of Supernovae, ed. A. W. Alsabti & P. Murdin, Vol. 375 (Berlin: Springer), 375
Jones, D. O., Riess, A. G., Scolnic, D. M., et al. 2018a, ApJ, 867, 108
Jones, D. O., Scolnic, D. M., Riess, A. G., et al. 2018b, ApJ, 857, 51
Kessler, R., Bassett, B., Belov, P., et al. 2010a, PASP, 122, 1415
Kessler, R., Becker, A. C., Cinabro, D., et al. 2009a, ApJS, 185, 32
Kessler, R., Bernstein, J. P., Cinabro, D., et al. 2009b, PASP, 121, 1028
Kessler, R., Conley, A., Jha, S., & Kuhlmann, S. 2010b, arXiv:1001.5210
Kessler, R., Guy, J., Marriner, J., et al. 2013, ApJ, 764, 48
Kessler, R., Narayan, G., Avelino, A., et al. 2019, PASP, 131, 094501
Kessler, R., & Scolnic, D. 2017, ApJ, 836, 56
Knights, M., Bassett, B. A., Varughese, M., et al. 2013, JCAP, 2013, 039
Komatsu, E., Dunkley, J., Nolta, M. R., et al. 2009, ApJS, 180, 330
Kunz, M., Bassett, B. A., & Hlozek, R. A. 2007, PhRvD, 75, 103508
Lampeitl, H., Smith, M., Nichol, R. C., et al. 2010, ApJ, 722, 566
Lasker, J., Kessler, R., Scolnic, D., et al. 2019, MNRAS, 485, 5329
Lochner, M., McEwen, J. D., Peiris, H. V., Lahav, O., & Winter, M. K. 2016, ApJS, 225, 31
Magee, M. R., Kotak, R., Sim, S. A., et al. 2016c, A&A, 589, A89
Möller, A., & de Boissière, T. 2020, MNRAS, 491, 4277
Perlmutter, S., Aldering, G., Goldhaber, G., et al. 1999, ApJ, 517, 565
Pierel, J. D. R., Rodney, S., Avelino, A., et al. 2018, PASP, 130, 114504
Planck Collaboration, Ade, P. A. R., Aghanim, N., et al. 2016a, A&A, 594, A13
Planck Collaboration, Ade, P. A. R., Aghanim, N., et al. 2016b, A&A, 594, A14
Riess, A. G., Filippenko, A. V., Challis, P., et al. 1998, AJ, 116, 1009
Roberts, E., Lochner, M., Fonseca, J., et al. 2017, JCAP, 2017, 036
Sako, M., Bassett, B., Becker, A., et al. 2008, AJ, 135, 348
Sako, M., Bassett, B., Becker, A. C., et al. 2018, PASP, 130, 064002
Sako, M., Bassett, B., Connolly, B., et al. 2011, ApJ, 738, 162
Scolnic, D., & Kessler, R. 2016, ApJL, 822, L35
Scolnic, D., Kessler, R., Brout, D., et al. 2018, ApJL, 852, L3
Smith, M., Bacon, D. J., Nichol, R. C., et al. 2014, ApJ, 780, 24
Stoughton, C., Lupton, R. H., Bernardi, M., et al. 2002, AJ, 123, 485
Stritzinger, M. D., Valenti, S., Hoeflich, P., et al. 2015, A&A, 573, A2
Sullivan, M., Conley, A., Howell, D. A., et al. 2010, MNRAS, 406, 782
Sullivan, M., Guy, J., Conley, A., et al. 2011, ApJ, 737, 102
Taylor, E. N., Hopkins, A. M., Baldry, I. K., et al. 2011, MNRAS, 418, 1587
The PLAsTiCC team, Allam, T. J., Bahmanyar, A., et al. 2018, arXiv:1810.00001
Villar, V. A., Berger, E., Metzger, B. D., & Guillochon, J. 2017, ApJ, 849, 70
Wolf, R. C., D'Andrea, C. B., Gupta, R. R., et al. 2016, ApJ, 821, 115
York, D. G., Adelman, J., Anderson, J. E., et al. 2000, AJ, 120, 1579